CCFE-PR(17)61

Jan Fikar, Robin Schäublin, Daniel R. Mason, and Duc Nguyen-Manh

Nano-size vacancy prismatic dislocation loops and vacancy clusters in tungsten

Nano-size vacancy prismatic dislocation loops and vacancy clusters in tungsten

Jan Fikar[a], Robin Schäublin[b], Daniel R. Mason[c], and Duc Nguyen-Manh[c]

[a]Central European Institute of Technology, Institute of Physics of Materials, Academy of Sciences of the Czech Republic, Žižkova 22, 616 00 Brno, Czech Republic

[b]Laboratory of Metal Physics and Technology, Department of Materials, ETH Zürich, 8093 Zürich, Switzerland

[c]CCFE, Culham Centre for Fusion Energy, Abingdon, Oxfordshire OX14 3DB, United Kingdom

Nano-size vacancy prismatic dislocation loops and vacancy clusters in tungsten

Jan Fikar[a,*], Robin Schäublin[b], Daniel R. Mason[c], Duc Nguyen-Manh[c]

[a] *Central European Institute of Technology, Institute of Physics of Materials, Academy of Sciences of the Czech Republic, Žižkova 22, 616 00 Brno, Czech Republic*
[b] *Laboratory of Metal Physics and Technology, Department of Materials, ETH Zürich, 8093 Zürich, Switzerland*
[c] *CCFE, Culham Centre for Fusion Energy, Abingdon, Oxfordshire OX14 3DB, United Kingdom*

Abstract

The vacancies produced in high energy collision cascades can form in irradiated tungsten vacancy clusters or vacancy prismatic dislocation loops. Moreover, vacancy loop can easily transform to a planar vacancy cluster. We investigated the formation energies of these three types of vacancy defects as a function of number of vacancies using three EAM tungsten potentials. The most favorable defect type and vacancy loop stability was determined. For very small sizes the planar vacancy cluster is more favorable than a vacancy loop, which is unstable. The void is the most stable vacancy defect up to quite large size, after that vacancy dislocation loop is more favorable. We however assume that the vacancy dislocation loops are nevertheless stable at low temperatures as the transformation to voids would need high temperature.

Keywords: prismatic dislocation loop, vacancy clusters, radiation damage, molecular statics, tungsten

1. Introduction

During high energy irradiation, lattice defects are produced in the form of interstitial- and vacancy- type point defects and clusters. In tungsten, recent simulations [1, 2] and experiments [3, 4] have shown that TEM visible nanoscale loops can be generated within the heat spike of a displacement cascade. The majority of these point defects mutually annihilates in the cascade cool down phase. While the surviving interstitials tend to form exclusively small interstitial prismatic dislocation loops, the surviving vacancies have more possibilities. They can create small prismatic dislocation loops or vacancy clusters. In fact, the large difference in formation energy of single interstitial and vacancy makes the interstitial cluster energetically very expensive. Traditionally it is assumed, that vacancies cluster together and are forming 3D voids in order to minimize the energy, while interstitials tend to cluster in planar objects, which collapse into energetically favorable prismatic dislocation loops. Here we focus on tungsten, one of the prime candidate material for the future fusion reactor.

In tungsten irradiated at low doses and moderate temperature transmission electron microscope (TEM) studies reveal the presence of prismatic dislocation loops with Burgers vectors $\frac{1}{2}\langle 1\,1\,1\rangle$ and $\langle 1\,0\,0\rangle$, the former dominating [5, 6]. TEM can in principle distinguish between interstitial and vacancy type loops using inside-outside contrast [7] if they are larger than about 4 nm, which corresponds to 220 point defects. For smaller loop it is difficult to distinguish its vacancy and interstitial nature, unless a dedicated TEM method based on diffuse scattering is applied [8]. Using the inside-outside contrast method some studies indicate vacancy type dislocation loops [5, 9–11] while other indicate interstitial type dislocation loops [6, 12] and some studies both [13]. Very recently, first-principles investigation in combination with Monte-Carlo simulations [14] showed that nano-size voids play important role for understanding the origin of anomalous precipitation of rhenium in neutron-irradiated tungsten at high temperature (900°C) [15].

In these irradiation conditions the voids in tungsten are mostly invisible in TEM as their size is below the TEM resolution of about 1 nm, but a post-irradiation anneal at 800°C for 1 hour reveals voids with a diameter of 1.5 nm, which corresponds approximately to 111 vacancies [6]. The TEM visibility limit of dislocation loop is also approximately 1 nm diameter, which corresponds to approximately 16 vacancies or interstitials.

The usual way to create a prismatic dislocation loop in simulations is to arrange the defects on a selected plane in a chosen shape. Relaxing such defect with interstitials leads to an interstitial prismatic dislocation loop, while the same defect created using vacancies can collapse to a vacancy prismatic loop or can remain stable as a planar vacancy platelet. Such uncollapsed 2D planar cluster of vacancies is sometimes called an open vacancy loop [16, 17], even though it is strictly speaking not a dislocation loop.

The prismatic dislocation loops behave in terms of mobility at smaller sizes more like a cluster of point defects, while at larger sizes they behave more like perfect prismatic dislocation loops [18]. Recent collision cascade simulations in tungsten reveal $\frac{1}{2}\langle 1\,1\,1\rangle$ and $\langle 1\,0\,0\rangle$ interstitial loops as well as $\langle 1\,0\,0\rangle$ vacancy loops [1].

The objective of this paper is to compare as a function of size three vacancy type defects of the same size, namely: (i) the vacancy prismatic dislocation loop, (ii) the planar vacancy platelet on the same habit plane as the corresponding loop and (iii) the 3D void. For comparison the interstitial prismatic dis-

*Corresponding author
Email address: fikar@ipm.cz (Jan Fikar)

location loop is also included.

2. Computational details

We consider a bulk-like cuboidal simulation block with periodic boundary conditions in all directions. The planar vacancy cluster is created by removing atoms on the plane {1 1 1} or {1 0 0}. In the case of {1 1 1} we consider the hexagonal shape and in the case of {1 0 0} the circular shape, as these are the shapes of lowest formation energies [19]. For small loop sizes the difference in circular and hexagonal shape is minimal. In fact, the hexagonal and circular loops are completely identical for sizes up to approximately 60 defects. The number of vacancies in the perfect hexagonal loop on {1 1 1} plane follows the simple sequence $N_i = 3i(i + 1) + 1$, where i is an integer. We investigated all the loops and clusters up to size 397, which corresponds to a diameter of 5.5 nm. Circular shape on the plane {1 0 0} yields a slightly different number of defects.

Because the dislocation loop creates a long-range deformation field, the dimensions of the simulation block should be at least 8 times the loop diameter to minimize the influence of the periodic images [20]. For the largest clusters and loops with 397 and 401 defects the simulation block has about 5.6 million atoms, corresponding to a box side of 40 nm.

The same procedure is applied to interstitials. After inserting or removing the defects, the simulation block is relaxed using the conjugate gradient method in LAMMPS [21] and the formation energy is calculated. The interstitial cluster collapses easily to the corresponding prismatic dislocation loop, but the planar vacancy cluster usually does not collapse. To create a vacancy dislocation loop we compress the sample unilaterally in the direction of the Burgers vector by 5-20%, then we relax the sample, cancel the compression and relax again. This simple procedure usually leads to a vacancy dislocation loop. If the amount of compression is too low, the vacancy cluster does not collapse. If the compression is too high, it produces completely disrupted sample. In general ⟨1 0 0⟩ needs higher compression, as the space between atoms due to the vacancy platelet is higher. Another possibility to create the vacancy loop is to move atoms closer after creating the vacancies. Then instead of one big gap between the atoms in the direction perpendicular to the defect plane we create three smaller gaps. Such samples usually collapse to dislocation loops without additional compression. The presence of a dislocation loop is examined by DXA algorithm in Ovito software [22]. Note that small ⟨1 0 0⟩ vacancy loops up to size 37 vacancies are not detected by DXA and manual investigation is needed. All the other types of loops are correctly detected by DXA. The 3D voids are simply created by selecting a sphere in the perfect sample, in which the atoms are discarded. For simplicity faceting is not taken into account.

In our atomistic simulations, we use three different EAM potentials: (i) the potential of Ackland and Thetford (*AT*) [23], (ii) the *EAM-4* potential developed in the paper by Marinica *et al.* [24] that we designate here as *M4*, and (iii) the recent potential of Mason, Nguyen-Manh and Becquart (*MNB*) [25], which is an improvement of *AT* potential. The *M4* potential predict incorrectly that ⟨1 0 0⟩ loops have lower formation energies than the corresponding ½⟨1 1 1⟩ loops for loops smaller than about 300 point defects, larger loops behave as expected [19]. The potentials *AT* and *MNB* predict the correct order of formation energies of ½⟨1 1 1⟩ and ⟨1 0 0⟩ loops. The main improvement of the *MNB* potential over previous EAM potentials is in better desciption of vacancy clusters and improved free surface energy. Previous potentials predict free surfaces energies lower by approximately 30% than the DFT and experimental values.

We fit the formation energy of the three different vacancy defects (hereafter the loop, the platelet and the void) as a functions of the number of included point defects N in the following way. The platelet can be approximated by a flat cylinder consisting of free surfaces with constant height

$$E_{platelet} = a_1 N + a_2 \sqrt{N}, \tag{1}$$

where N is proportional to the surface of the two circular faces of the cylinder, $\sqrt{N}$ is proportional to its circumference, and a_1 and a_2 are fitting parameters. With a_1 we can calculate the free surface energy in the direction perpendicular to the platelet habit plane

$$\gamma_{111} = \frac{\sqrt{3} a_1}{2 a_0^2} \tag{2}$$

for the {1 1 1} platelet and

$$\gamma_{100} = \frac{a_1}{a_0^2} \tag{3}$$

for the {1 0 0} platelet. The fitting constant a_2 is a product of the small cylinder height and an average free surface energy in the directions in the defect plane.

The 3D spherical void formation energy can be approximated as a average free surface energy multiplied by the void surface

$$E_{void} = b_1 N^{2/3}. \tag{4}$$

The average free surface energy γ_a can be calculated from the only fitting parameter b_1

$$\gamma_a = \frac{b_1}{\sqrt[3]{9\pi} a_0^2}. \tag{5}$$

The prismatic dislocation loop formation energy can be fitted with the formula [19]

$$E_{loop} = R_c b^2 \left(c_1 + c_2 \ln R_c\right), \tag{6}$$

where b is the Burgers vector amplitude, c_2 can be determined from elastic constant and for tungsten $c_2 = \mu/(2(1-\nu))$=22.41 eVa_0^{-3}, R_c is equivalent loop radius and c_1 is the only fitting parameter related to the dislocation core. The equivalent loop radius can be expressed from number of defects N as

$$R_c = a_0 \sqrt{\frac{N}{\sqrt{3}\pi}} + \Delta R_{core}, \tag{7}$$

for ½⟨1 1 1⟩ and

$$R_c = a_0 \sqrt{\frac{N}{2\pi}} + \Delta R_{core}, \tag{8}$$

for ⟨1 0 0⟩. The dislocation core position correction ΔR_{core} is important especially for small loops. It is positive for interstitial type loops and negative for vacancy type loops. We use the values $a_0/(2\sqrt{6})$ and $a_0/4$ for ½⟨1 1 1⟩ and ⟨1 0 0⟩, respectively.

3. Results and discussion

The formation energies divided by number of defects E_f/N of the vacancy clusters and dislocation loops are reported in Figs. 1,2 and 3 for potential *AT*, *M4* and *MNB*, respectively. The formation energy for the void as a function of size shows a larger scatter, which is probably caused by the lack of faceting. Indeed, in reality the void surfaces will be faceted in ⟨1 1 0⟩ directions, where the surface energy has a minimum. As a result we expect the faceted void to have a lower formation energy. However, our spherical void shape allows us calculating a more precise average free surface energy γ_a, which is for *MNB* potential very close to the experimental value, see table 1.

The platelet formation energy is for small sizes lower than the energy of the loop. From a certain critical size $N_{platelet}$ the loop is energetically more favorable than the platelet. With an increasing number of the defects N the platelet formation energy per defect E_f/N decreases only slightly and tends asymptotically to a constant for large sizes. The distance of the atoms across the platelet is 4.47 and 5.24 Å for the {1 1 1} and {1 0 0}, respectively, which is in some cases lower than the range r_{cut} of the potentials 4.50, 5.50 and 4.40 Å for *AT*, *M4* and *MNB*, respectively. Despite that the Eq. 1 can be used to calculate precise surface energies for {1 1 1} or {1 0 0} surfaces, see table 1. The uncollapsed vacancy planar clusters can thus be approximated by a flat cylinder of free surfaces with constant height. If we approximate the average free surface energy by the sphere value derived from Eq. 5 we can estimate the cylinder height. It is $0.2a_0$–$0.3a_0$ and $0.4a_0$–$0.6a_0$ for the {1 1 1} and {1 0 0} platelet, respectively.

The formation energy per defect of the vacancy dislocation loop decreases with N as the loop formation energy for large loops should increase as its circumference $\sqrt{N}$ see Eq. 6. Also the formation energies for interstitial and vacancy type loops should be close to each other for large sizes, as for large diameters the ΔR_{core} can be neglected. Thus, for sizes up to a critical size $N_{platelet}$ it is more favorable for the vacancies to remain as a platelet, while for larger sizes it collapses into a dislocation loop. The critical sizes for the studied potentials are summarized in table 2.

The critical sizes $N_{platelet}$ are in general higher for ⟨1 0 0⟩ loops when compared to ½⟨1 1 1⟩ loops. When we compare the different potentials, the critical sizes $N_{platelet}$ are lowest for *MNB* potential due to higher free surface energies. Only this potential predicts the nanometric vacancy loop as more stable than the platelet. The *M4* potential does not allow stable small vacancy loops; such a loop upon relaxation bulge out and ends as a platelet. This is observed for sizes 7 and 19 in ½⟨1 1 1⟩ and for sizes 9, 21 and 37 in ⟨1 0 0⟩.

Similar approach for ½ ⟨1 1 1⟩ vacancy loops in tungsten using *DND* potential [26] gives $N_{platelet}$=157 [16], which is significantly higher than for the three potentials investigated here.

Table 1: The free surface energies γ_{111} and γ_{100} calculated by fitting Eq.1 to platelets and an average free surface energy γ_a calculated by fitting Eq.4 to voids. The values in brackets are from [25]. Note the average experimental value is 0.229 eVÅ^{-2} [27].

	AT	*M4*	*MNB*
γ_{111} [eVÅ^{-2}]	0.206 (0.206)	0.203 (0.200)	0.259 (0.257)
γ_{100} [eVÅ^{-2}]	0.182 (0.182)	0.183 (0.183)	0.240 (0.239)
γ_a [eVÅ^{-2}]	0.181	0.181	0.230

Table 2: The critical size $N_{platelet}$ (interpolated) from which a vacancy dislocation loop is more favorable than a platelet and the critical size N_{void} (extrapolated using Eqs. 4 and 6) from which a vacancy dislocation loop is more favorable than a void. The corresponding loop d_{loop} and void d_{void} diameters are indicated.

	AT	*M4*	*MNB*
$N_{platelet}$ ½⟨1 1 1⟩	30	115	14
d_{loop} [nm]	1.49	2.91	1.02
$N_{platelet}$ ⟨1 0 0⟩	136	283	46
d_{loop} [nm]	2.95	4.25	1.71
N_{void} ½⟨1 1 1⟩	7.86×10^5	2.59×10^6	5.82×10^4
d_{loop} [nm]	241	437	65
d_{void} [nm]	28.8	42.8	12.1
N_{void} ⟨1 0 0⟩	4.93×10^6	1.09×10^7	6.31×10^5
d_{loop} [nm]	561	834	201
d_{void} [nm]	53.0	69.1	26.7

Results are summarized in table 2. The voids have the lowest formation energies in all studied cases, but as their energy increases with the number of defect as $N^{2/3}$ (Eq. 4), they should at some point N_{void} intersect with the large loops, whose formation energy follows $\sqrt{N}$ (Eq. 6). Using our fitted curves we can extrapolate and find these critical sizes N_{void}. For sizes larger than N_{void} the vacancy prismatic dislocation loops are the most energetically favorable defects. The resulting values of N_{void} are really high. The same applies here as for $N_{platelet}$: the critical sizes are higher for the ⟨1 0 0⟩ loops when compared to the ½⟨1 1 1⟩ loops and *MNB* potential gives the lowest critical sizes due to higher free surface energies.

There is a difference though as the transformation path between the platelet and the loop is easy being diffusionless, as it involves just a slight movement of couple of the atoms in the middle of the disc, while the transformation between a 3D void and a vacancy dislocation loop involves diffusion with the movement of many atoms. The latter would require high temperatures to allow for the required diffusion.

4. Conclusions

We have investigated the formation energies of three different vacancy defects (the dislocation loop, the platelet and the void) and compared them to the interstitial dislocation loop by employing atomistic simulations and three EAM potentials. The most suitable potential for vacancy type defects appears to be *MNB* potential, which predicts correct free surface energies. The formation energies of the defect clusters are successfully

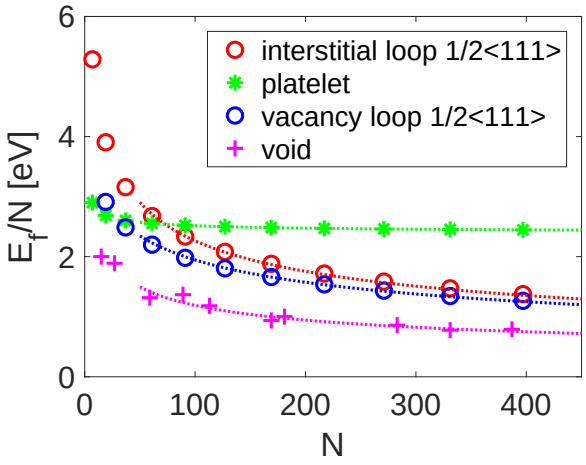

(a)

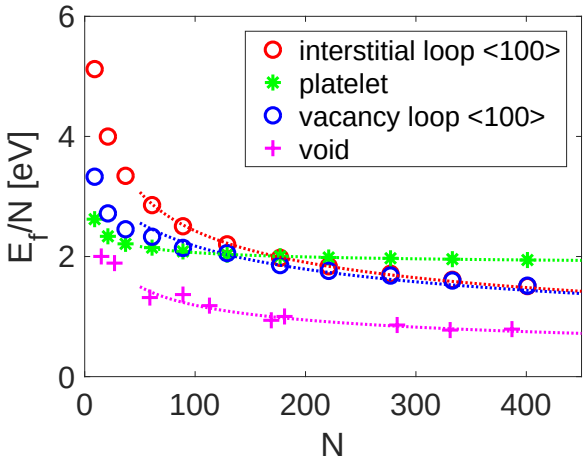

(b)

Figure 1: Dependence of the formation energy divided by number of defects E_f/N on the number of defects N for vacancy and interstitial dislocation loops, platelet and void calculated using *AT* potential (a) on the {1 1 1} plane and (b) on the {1 0 0} plane. The dotted lines are the fits using Eqs. 1, 4 and 6.

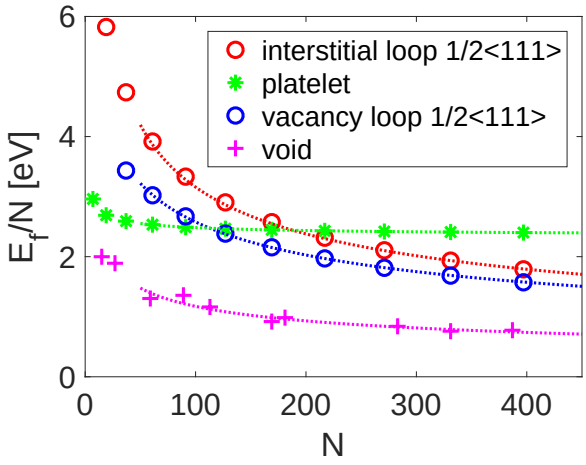

(a)

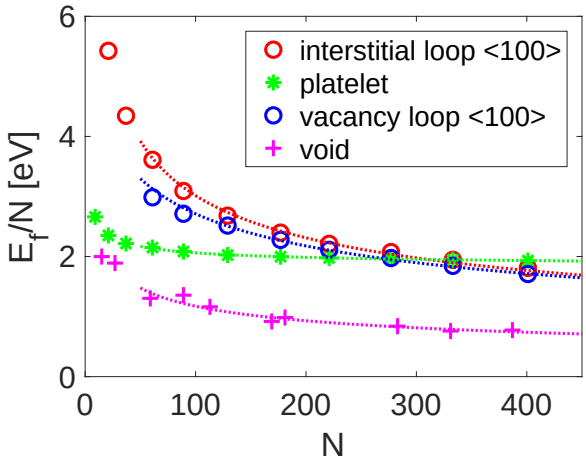

(b)

Figure 2: Dependence of the formation energy divided by number of defects E_f/N on the number of defects N for vacancy and interstitial dislocation loops, platelet and void calculated using *M4* potential (a) on the {1 1 1} plane and (b) on the {1 0 0} plane. The dotted lines are the fits using Eqs. 1, 4 and 6.

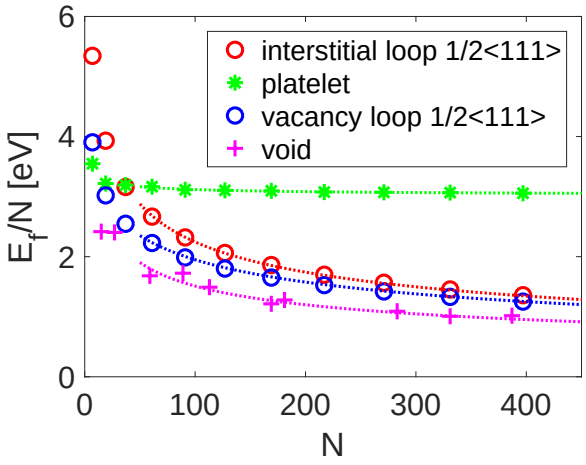

(a)

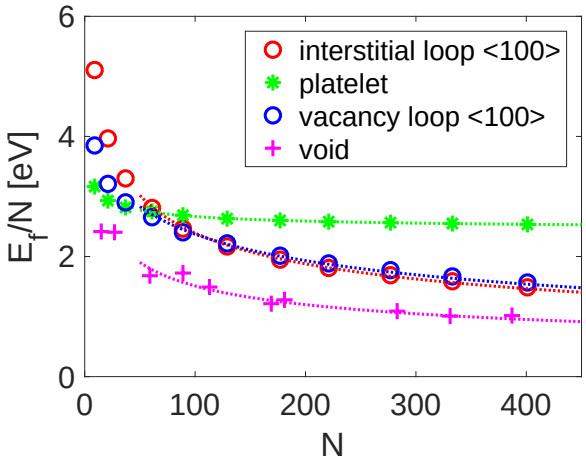

(b)

Figure 3: Dependence of the formation energy divided by number of defects E_f/N on the number of defects N for vacancy and interstitial dislocation loops, platelet and void calculated using *MNB* potential (a) on the {1 1 1} plane and (b) on the {1 0 0} plane. The dotted lines are the fits using Eqs. 1, 4 and 6.

fitted by simple formulas using just one or two fitting parameters. Our specific conclusions are the following:

The platelet is stable up to a critical size of 14 and 46 vacancies, which corresponds to a diameter of 1.0 and 1.7 nm for the ½⟨1 1 1⟩ and ⟨1 0 0⟩ loop, respectively, as predicted by *MNB* potential. For larger sizes we expect it to collapse fairly easily to a vacancy prismatic dislocation loops.

The voids have the lowest formation energies up to a critical size of 6×10^4 and 6×10^5 vacancies, which corresponds to a loop diameter of 65 and 200 nm and a void diameter of 12 and 27 nm for the ½⟨1 1 1⟩ and ⟨1 0 0⟩ loop, respectively, as extrapolated using *MNB* potential. The transformation from the void to the platelet and vice versa is however not straightforward and involves diffusion for the needed movement of many atoms, so we expect high temperatures for this to occur.

The other investigated potentials underestimate the free surface energies by approximately 30% and as a result the platelet and the void are favored when compared to the vacancy dislocation loop. This leads to higher critical sizes and makes the small vacancy loop less stable.

Acknowledgments

This work was supported by the Grant Agency of the Czech Republic, Grant No. 16-24402S. This research was carried out under the project CEITEC 2020 (LQ1601) with financial support from the Ministry of Education, Youth and Sports of the Czech Republic under the National Sustainability Program II. Access to computing and storage facilities owned by parties and projects contributing to the National Grid Infrastructure MetaCentrum, provided under the program "Projects of Large Research, Development, and Innovations Infrastructures" (CESNET LM2015042), is greatly appreciated. DRM and DNM would like to acknowledge funding from Euratom research and training programme 2014–2018 under grant agreement number No. 633053, and funding from the RCUK Energy Programme (Grant Number EP/P012450/1). The views and opinions expressed herein do not necessarily reflect those of the European Commission.

References

[1] A. E. Sand, S. L. Dudarev, K. Nordlund, EPL (Europhysics Letters) 103 (4) (2013) 46003.
[2] A. E. Sand, D. R. Mason, A. D. Backer, X. Yi, S. L. Dudarev, K. Nordlund, Materials Research Letters 5 (5) (2017) 357–363.
[3] X. Yi, A. E. Sand, D. R. Mason, M. A. Kirk, S. G. Roberts, K. Nordlund, S. L. Dudarev, EPL (Europhysics Letters) 110 (3) (2015) 36001.
[4] D. R. Mason, A. E. Sand, X. Yi, S. L. Dudarev, Acta Materialia.
[5] D. R. Mason, X. Yi, M. A. Kirk, S. L. Dudarev, J. Phys.-Condens. Mat. 26 (37) (2014) 375701.
[6] F. Ferroni, X. Yi, K. Arakawa, S. P. Fitzgerald, P. D. Edmondson, S. G. Roberts, Acta Mater. 90 (2015) 380–393.
[7] H. Föll, M. Wilkens, physica status solidi (a) 31 (2) (1975) 519–524.
[8] M. A. Kirk, M. L. Jenkins, Z. Zhou, R. D. Twesten, A. P. Sutton, S. L. Dudarev, R. S. Davidson, Philosophical Magazine 86 (29–31) (2006) 4797–4808.
[9] R. C. Rau, Philos. Mag. A 18 (155) (1968) 1079–1084.
[10] W. Jäger, M. Wilkens, physica status solidi (a) 32 (1) (1975) 89–100.

[11] X. Yi, M. L. Jenkins, M. A. Kirk, Z. Zhou, S. G. Roberts, Acta Mater. 112 (2016) 105 – 120.
[12] Y. Watanabe, H. Iwakiri, N. Yoshida, K. Morishita, A. Kohyama, Nuclear Instruments and Methods in Physics Research Section B: Beam Interactions with Materials and Atoms 255 (1) (2007) 32 – 36.
[13] X. Yi, M. L. Jenkins, M. Briceno, S. G. Roberts, Z. Zhou, M. A. Kirk, Philos. Mag. 93 (2013) 1715–1738.
[14] J. S. Wrobel, D. Nguyen-Manh, K. J. Kurzydlowski, S. L. Dudarev, J. Phys.: Condensed Matter 29 (2017) 154403.
[15] M. Klimenkov, U. Jantsch, M. Reith, H. C. Scheneider, D. J. H. Armstrong, J. Gibson, S. R. Roberts, Nucl. Mater. Energy 9 (2016) 480.
[16] M. R. Gilbert, S. L. Dudarev, P. M. Derlet, D. G. Pettifor, Journal of Physics: Condensed Matter 20 (34) (2008) 345214.
[17] M. R. Gilbert, Z. Yao, M. A. Kirk, M. L. Jenkins, S. L. Dudarev, Journal of Nuclear Materials 386-388 (2009) 36–40.
[18] P. M. Derlet, M. R. Gilbert, S. L. Dudarev, Phys. Rev. B 84 (2011) 134109.
[19] J. Fikar, R. Gröger, Solid State Phenom. 258 (2017) 97–101.
[20] J. Fikar, R. Schäublin, Nucl. Instrum. Meth. B 267 (2009) 3218–3222.
[21] S. Plimpton, J. Comp. Phys. 117 (1995) 1–19.
[22] A. Stukowski, V. V. Bulatov, A. Arsenlis, Model. Simul. Mater. Sc. 20 (8) (2012) 085007.
[23] G. J. Ackland, R. Thetford, Philos. Mag. A 56 (1987) 15–30.
[24] M.-C. Marinica, L. Ventelon, M. R. Gilbert, L. Proville, S. L. Dudarev, J. Marian, G. Bencteux, F. Willaime, J. Phys.-Condens. Mat. 25 (39) (2013) 395502.
[25] D. R. Mason, D. Nguyen-Manh, C. S. Becquart, J. Phys.: Condens. Matter 29 (2017) 505501.
[26] P. M. Derlet, D. Nguyen-Manh, S. L. Dudarev, Phys. Rev. B 76 (2007) 054107.
[27] F. de Boer, R. Boom, W. Mattens, A. Miedema, A. Niessen, Cohesion in Metals, Amsterdam: North-Holland, 1988.